JOURNAL OF PROPULSION AND POWER
Vol. 24, No. 2, March–April 2008

Examination of a Collision-Limiter Direct Simulation Monte Carlo Method for Micropropulsion Applications

E. Titov,* A. Gallagher-Rogers,† and D. Levin‡
Pennsylvania State University, University Park, Pennsylvania 16802
and
Brian Reed§
NASA John H. Glenn Research Center at Lewis Field, Cleveland, Ohio 44135

DOI: 10.2514/1.28793

A wide range of flow regimes occur in micronozzles, from the transitional to the continuum regime, which prevents the use of a single computational method such as direct simulation Monte Carlo or computational fluid dynamics and Navier–Stokes. A collision-limiter approach is proposed that extends the applicability of direct simulation Monte Carlo to the continuum regime and can be used to solve a wide range of microelectromechanical system flows when it is coupled with the baseline direct simulation Monte Carlo. A comparison of the results obtained with this computational technique with new experimental data and Navier–Stokes results suggests consistency between experimental and computational methods for three-dimensional microelectromechanical system micronozzles with stagnation pressures on the order of 5 atm. However, the level of agreement was found to vary with the nozzle geometry, suggesting that additional research is needed for both computations and experiments in this flow regime.

Nomenclature

C	=	velocity of molecules, components are C_x, C_y, and C_z
$f(C)$	=	distribution function of the molecular velocities
f_0	=	equilibrium distribution function
i, j, k	=	Cartesian coordinate indexes
K	=	heat transfer coefficient
k	=	Boltzmann constant
m	=	mass of the molecule
P	=	pressure
q_i, qx, qy, qz	=	heat flux components
T	=	temperature
U	=	flow velocity (the absolute value)
x, y, z	=	Cartesian coordinates
Γ	=	deviation of the distribution function from the Maxwellian
δ_{ij}	=	equal to 0 when $i = j$ and 1 otherwise
μ	=	viscosity coefficient
$v_i, v_j v_k, Ux, Uy, Uz$	=	flow velocity components
$\tau_{i,j}, \tau_{xx}, \tau_{xy}$	=	shear stress tensor components

I. Introduction

NEW microelectromechanical systems (MEMS)-based micropropulsion systems capable of delivering precise impulses for small spacecraft maneuvers have been recently developed [1]. The advantages of MEMS-based micropropulsion devices include weight reduction through the use of lightweight materials, the ability to provide versatile thrust levels, and the potential for using such devices to permit microsatellite constellation clustering [2]. Micronozzle devices will operate over a range of pressures, from approximately 0.1 to 6 atm, with the actual stagnation pressure depending on the specific mission requirements. The higher pressure limit may be more challenging from a fabrication point of view, but the physics of the micronozzle flow indicates that there will be a significant improvement in propulsion device performance. As micronozzle concepts and designs evolve, the availability of reliable modeling and simulation to predict and improve system performance is crucial. The small device size, as well as the two- and three-dimensional geometries chosen to permit micronozzle clustering for performance enhancement, leads to a relatively large surface-to-volume ratio of MEMS micronozzles. These conditions create a micronozzle flow that is highly viscous and challenging to model. In this paper, we present the application of a computational technique related to direct simulation Monte Carlo (DSMC) collision-limiter schemes and use it to analyze new thrust measurements of three-dimensional micronozzles.

Although the application of MEMS micropropulsion devices promises technological advances for space vehicles, there is still a paucity of available experimental data. Of the data that have been obtained, we briefly review some of the key contributions. In the work of Ketsdever et al. [3], experiment and DSMC computations were compared for a micronozzle and an orifice with lower stagnation-pressure values than will be considered here and Reynolds numbers in the range from ~0 to 22. The research showed the trends in the device performance along with increase in the stagnation pressure from the free-molecular regime ($Kn \sim 50$) through the continuum regime ($Kn \sim 0.005$). It was demonstrated that for the lower pressure levels, the performance of the orifice is better than that of a nozzle due to the thick boundary layer forming in the diverging potion of the nozzle and that the continuum approaches poorly predict the device performance for lower pressure levels. Viscous effects in the supersonic MEMS micronozzles were also studied by Bayt and Breuer [4], who experimentally analyzed four different nozzles with aspect ratios ranging from 5.4:1 to 17:1 and Reynolds numbers ranging from 500 to 3500. It was shown in that work that supersonic flow can be achieved in micron-scale nozzles with a throat height on the order of 20 μm and the thrust efficiency for this geometry was presented. In [5], higher stagnation-pressure levels (up to 10 atm) were considered for micronozzle configurations. For Reynolds numbers larger then 2300,

Received 9 November 2006; revision received 18 July 2007; accepted for publication 13 September 2007.

*Graduate Student, Department of Aerospace Engineering. Student Member AIAA.
†Graduate Student, Department of Aerospace Engineering.
‡Associate Professor, Department of Aerospace Engineering. Associate Fellow AIAA.
§Aerospace Engineer, Electric Propulsion Branch, Mail Stop 301-3. Member AIAA.

experimental mass flow and thrust efficiency values were compared with turbulent computational fluid dynamics (CFD) solutions. However, for these cases, the background pressure was on the order of 1 atm and the formation of shock waves in the computed flow was observed and studied. The thrust data that will be presented in this paper and compared with modeling and simulation are obtained for near-vacuum background conditions, similar to what would be experienced for satellite applications.

In this paper, we present a range of experimental data obtained on micronozzles with area ratios between 1 and approximately 18.4 for five different nozzle configurations. Thrust data were measured for stagnation temperatures varied from 292 to 734 K, but, stagnation pressure was kept relatively constant at a level of 4.5 to 6.5 atm. The flow regimes studied correspond to the current demand to increase the performance of the micronozzles by increasing the stagnation pressure to high levels. The thrust measurements and modeling of the microdevices to be discussed in this work show that for stagnation pressures on the order of 5 atm, an increase in the stagnation temperature does not lead to better performance, as might be expected. Increase in the stagnation temperature has the effect of making the flow more viscous and thereby lowering the efficiency of the nozzle for this relatively low Reynolds number regime.

The modeling of micronozzle low Reynolds number supersonic flows has been an active area of research for the last few years. In the research of Bayt and Breuer [4], finite volume Navier–Stokes (NS) simulations were performed for two-dimensional nozzles. At sufficiently low Knudsen numbers, several DSMC computations have been performed for different micronozzle geometries [6–10]. In our previous research [8–10], we emphasized the study of three-dimensional high-aspect-ratio nozzles with the DSMC technique. The thrust losses were found to be greater for this geometry relative to an axisymmetric conical-shaped nozzle, and the flow structure and thrust were found to be coupled to the thermal material response [9,10]. In this paper, we consider extending the modeling regime to higher stagnation-pressure levels, an operating regime in which, in general, the performance of the MEMS micronozzle will improve.

Because a wide range of flow regimes occur in micronozzles, from the transitional to the continuum regime, it is not likely that a single computational method, such as DSMC or CFD/NS, can be successfully used to model the entire flow. In previous work [11], we presented an analysis of the numerical errors that are present in the results of DSMC applied to a three-dimensional micronozzle with a stagnation pressure on the order of 0.1 atm. The analysis shows that the lowest-pressure case that is applicable to practical MEMS micronozzles is also the highest-pressure case that the baseline DSMC can reliably model. Extensions to higher-pressure cases might be possible, based on an analysis of the deterministic errors in the solution. However, it is unlikely that such a technique would provide a robust solution at higher pressures, because one must first demonstrate that the errors are in a linear regime. In addition, for stagnation pressures on the order of 0.1 to 1 atm, the use of the Navier–Stokes equations to accurately model the large boundary layer is still problematic.

Because of the continuing challenges of modeling micronozzle flows in the 200 to 2000 Reynolds number regime, a numerical technique is proposed to model operational three-dimensional micronozzles. The method, designated in this paper as eDSMC, extends the DSMC technique to high-pressure flows and is based on the collision-limiter schemes considered in the past. The distinction of the proposed eDSMC method is that based on presimulation testing, local equilibrium is assumed to have occurred after a fixed number of collisions per time step per cell. We use the term *collision-limiter* in this paper in a slightly different manner from that originally suggested by Lengrand et al. [12]. Unlike Lengrand et al., we do not calculate the real collision frequency of molecules in the computational cells. Instead, we estimate the required number of collisions per particle necessary to establish local equilibrium and then force particles to perform this number of collisions. To test the method with standard DSMC and NS methods, axisymmetric nozzle and embedded-channel flows were simulated and compared with experimental temperature data and preexisting calculations, respectively, in [13,14]. The method was shown to be accurate for inviscid flows, and Chapman–Enskog theory was used to predict the range of initial conditions in which eDSMC is likely to be useful for viscous flows. For supersonic expansion from an axisymmetric nozzle, the proposed method was coupled with the baseline DSMC method to capture the varying physics and length scales in the flow. The hybrid approach was found to be more efficient than DSMC, wherein the majority of the computational effort is invested in generating a large sample size to adequately characterize the velocity distribution functions, even in the regions in which the distribution function is known to be Maxwellian. The development of a hybrid DSMC/eDSMC method increases the range of stagnation conditions possible for simulating high-pressure expanding flows into space for near-vacuum conditions.

The purpose of this paper is twofold. One goal of this work is to establish the utility of the eDSMC numerical technique [11] as a separate standalone method, by comparison with a known computational technique, NS. The second goal of the paper is to present new higher-pressure and higher-temperature micronozzle thrust data for a range of area ratios and stagnation conditions. Modeling and simulation will be used to analyze the influence of the nozzle configuration and stagnation conditions on the measured nozzle performance trends. The remainder of the paper is organized as follows. In Sec. III, we discuss the proposed extension of the DSMC method, which includes the implementation of the collision-limiter method and the theory of establishing the extent of local equilibrium in the flow through the use of the Komogorov–Smirnov test and Chapman–Enskog pertubation theory. In Sec. IV, we compare the proposed eDSMC method against NS results and show that the level of agreement between the two computational methods is consistent with the values of the Chapman–Enskog-derived heat flux and shear stress tensor quantities. Finally, in Sec. V, we describe the testing and measurement of the micronozzles, present the data, and compare eDSMC flowfield simulations and thrust levels for selected cases. The trends in the data are presented and the comparison of modeling and simulation with a portion of the data show consistency between modeling and data. Most of the eDSMC simulations agree well with the measured thrust values for one of the shorter nozzle configurations. However, for a longer micronozzle geometry, we show that because the internal nozzle flow is completely subsumed by the boundary layer viscous flow, both eDSMC and NS may have difficulty predicting the measured thrust. The limitations of the experimental data, particularly with respect to measurement of the fabricated nozzle geometries, are also discussed and potentially affect the comparisons of both eDSMC and NS with data.

II. Proposed Extension of DSMC Method: eDSMC

The DSMC method of Bird [15] is a statistical approach used to solve the Boltzmann equation, which describes the discrete nature of rarefied gases. The correct usage of the DSMC method requires time and space discretization by sufficiently small quantities to ensure that the predicted flow parameters correspond to a solution of the Boltzmann equation. Furthermore, these numerical parameters may be adaptive to the flow gradients, but one must still use a sufficient number of computational particles per cell to obtain a physically reasonable result (i.e., correctly reproduce the true collision frequency) even when grid adaptation is available.

For the higher pressure levels, an equilibrium version of the DSMC technique is considered in this work. The idea of using the DSMC method for inviscid continuum flows was first introduced by Pullin [16]. Recently, Macrossan et al. [17] developed and tested a new method that is based on Pullin's [16] idea, but uses a conventional finite volume representation and a particle approach for modeling the transport of mass, momentum, and energy fluxes from cell to cell. A different approach, introduced by Lengrand [12], is based on the idea of limiting the number of collisions in a cell by a specific number of collisions per particle. The basic idea of the collision-limiter is to limit the number of collisions per particle when further collisions do not change the local distribution function.

In this paper, we use a different definition of the collision-limiter. We define the collision-limiter as the number of collisions necessary to create a local Maxwellian distribution of molecular velocities by providing a sufficient number of collisions to ensure thermal velocity relaxation in each computational cell and for each time step. We denote the proposed scheme as eDSMC to emphasize that local equilibrium is the only assumption in the scheme. Unlike the usual DSMC scheme, when we implement eDSMC, we do not try to reproduce the true kinetic collision frequency per cell. Instead, we collide a particle a fixed number of times per time step, such that the number of collisions per particle will be, on average, equal to the collision-limiter. Following the work of Sharma and Long [18], we use a value of the limiter equal to two, and in previous work, we also verified that this is an adequate value for micronozzle flows [13]. The use of a collision-limiter scheme allows us to use larger cells and time steps than would be possible with the baseline DSMC method, thereby reducing the eDSMC computational cost. The eDSMC algorithm has the following steps:

1) Select particles in each cell.

2) Loop over the cells.

3) For each of the cells, implement $2N$ collisions, where N is the number of particles in the cell and the value of 2 is the collision-limiter. The pairs are chosen according to the acceptance-rejection technique.

4) Introduce the new particles into the system according to the boundary conditions at the inlet and outlets.

5) Move all of the particles in the system, implementing the boundary conditions at the walls.

6) Sample the distributions for the macroparameters.

III. Comparison of eDSMC Against a Three-Dimensional MEMS Nozzle NS Solution

The NS and eDSMC calculations were performed for case I ($P_o = 5$ atm). Table 1 provides the specific geometry for the case, and Fig. 1 presents the schematics of the 3D computational domain used in this and subsequent calculations for this case. Table 2 provides the numerical parameters and conditions for the eDSMC calculations. The subsonic portion of the nozzle was modeled to provide a better approximation of the flow parameters at the entrance into the supersonic portion of the nozzle (the region of main interest), rather than calculating the sonic boundary conditions at the end of the throat by the isentropic theory. All of the results in this paper present the supersonic portion of the nozzle, starting from the end of the nozzle throat, which is 0.25 mm in length. With small modifications, the same computational domain was used for both eDSMC and NS solvers. We made use of the two symmetry planes existing in the problem, which allowed us to solve for one-quarter of the domain. A downstream subdomain was attached to the nozzle exit to make sure that the downstream boundary conditions are set away from the nozzle exit.

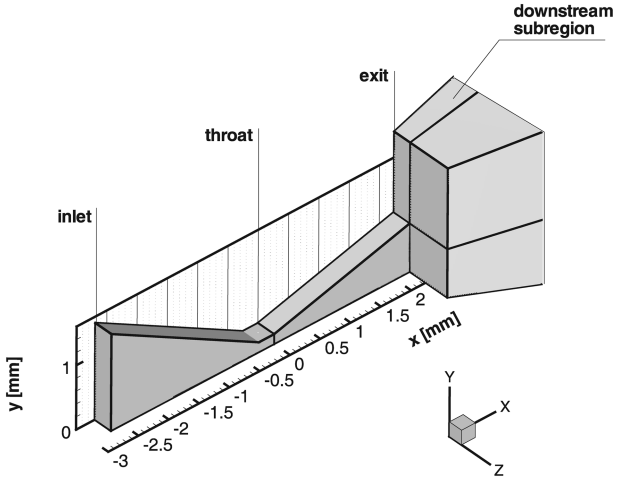

Fig. 1 Schematic of the computational domain for eDSMC and NS calculations.

Table 1 Flow and nozzle conditions[a,b,c,d,e]

	Case I	Case II	Case III	Case IV	Case V	Case VI	Case VII
Length[a]	2.44	2.21	2.21	2.21	2.21	2.21	4.49
Inlet height	3.0	3.0	3.0	3.0	3.0	3.0	3.0
Throat height	0.3	0.24	0.24	0.24	0.24	0.24	0.33
Exit height	1.5	1.4	1.4	1.4	1.4	1.4	2.98
Depth	1.2	2.52	2.52	2.52	2.52	2.52	2.49
Area ratio	4.0	5.83	5.83	5.83	5.83	5.83	9.03
Stagnation pressure, atm	5	5.10	5.24	5.65	5.17	5.44	5.65
Stagnation temperature, K	2000	292	399	484	583	657	727
Exit Mach number [b]	3.2	3.35	3.35	3.35	3.35	3.35	3.82
Reynolds number	3960	34,390	23,680	20,121	14,722	13,457	16,522
Knudsen number	0.0004	0.000043	0.000062	0.000074	0.00010	0.00017	0.00008
Gas	Ar	N2	N2	N2	N2	N2	N2
Nozzle type	Figure 1	5-A	5-A	5-A	5-A	5-A	10-A

[a]The nozzle dimensions are given in millimeters.
[b]Derived from isentropic theory.
[c]Background pressure ~ zero.
[d]Internal degrees of freedom were frozen for cases II–VII.
[e]Characteristic size is the hydraulic diameter of the throat: 4 × area/perimeter.

Table 2 eDSMC computational parameters[a]

Case	Number of computational particles	Number of cells	Gas–surface boundary condition	Computed thrust, N	Measured thrust, N
I	69,439,112	82,722,384	Adiabatic		
II	17,685,500	19,157,480	Thermal	0.343	0.383
III	15,212,465	16,670,751	Thermal	0.340	0.400
IV	13,919,939	15,356,119	Thermal	0.364	0.405
V	11,972,523	13,399,793	Thermal	0.330	0.343
VI	11,166,929	12,570,745	Thermal	0.346	0.356
VII	11,815,313	14,066,317	Thermal	0.592	0.460

[a]The time step and collision-limiter values are 2 ns and two collisions per time step per cell, respectively.

Note that we considered argon as a working gas in this case to eliminate the influence of the internal degrees of freedom in the comparison between the eDSMC and NS results. A stagnation temperature of 2000 K was chosen for this case, similar to conditions studied previously [9,10]. Several eDSMC calculations have been done, with the most intensive ones taking about two days to perform on a cluster of 54 AMD 1.5-GHz processors. The numerical solution of the Navier–Stokes equations for viscous flow was obtained by use of the GASP [19] software, which uses a finite volume discretization of the computational domain. A no-slip adiabatic boundary condition was used to model the gas–surface interaction. Studies of the influence of different boundary conditions on the nozzle flow parameters can be found in earlier work [20]. The 3D structural mesh was created and optimized using the GRIDGEN [21] software to resolve the flow gradients, and several steps of mesh refinement were performed. The entire computational domain was divided into a number of zones, and different meshing strategies were used for each particular zone. Special attention was paid to meshing the boundary-layer zones and nozzle-lip zones, in which the flow gradients are expected to be maximal. The mesh structure was manually adapted following the flow gradients predicted by each run of the numerical procedure to ensure grid convergence.

It was found that the eDSMC solutions typically required approximately a factor of 1.5 longer computation times than a NS solution, if careful NS simulation conditions were fulfilled to prevent divergence of the solution. The initial meshing was performed in eDSMC using an automated procedure to generate a simple orthogonal grid. As mentioned previously, to obtain a suitable grid for the NS calculations, 12 zones were created (with nine for the boundary-layer region) inside the three-dimensional nozzle and four zones were created downstream of the nozzle exit to enable a one-to-one correspondence between the internal and external zones. The eDSMC calculations used a stagnation subsonic boundary condition and a vacuum boundary condition at the inlet and outlet, respectively. The NS solutions used a Riemann boundary condition at the inlet and pressure boundary condition at the outlet and required iterations to gradually decrease the outlet pressure level sufficiently slowly to maintain a stable solution. With respect to mesh adaptation, the procedure used in eDSMC was to automatically adjust mesh size using a local density gradient criteria. In the NS calculations, the grid was manually adapted based on analyses of the previously obtained solutions. So although an unoptimized eDSMC is computationally slower than NS in terms of practical run time, a typical eDSMC solution took about two days (once submitted), whereas a NS solution took about three to four days, with half of the time spent on setting up the case and the other half running a constantly monitored solver.

To understand the likelihood that eDSMC will be useful, we need to estimate the degree of deviation of the flowfields of interest from Maxwellian. The NS calculations are considered to be exact and serve to validate the eDSMC for the high-pressure case I. Because velocity distributions are not given by NS, we use the local equilibria criteria, Chapman–Enskog theory, to provide the theoretical justification for the application of eDSMC for this and subsequent high-pressure cases discussed in this paper. We make use of the distribution function $f(C)$, given by Eq. (1):

$$f(C) = f_o(C)\Gamma(C) = \frac{1}{\pi^{\frac{3}{2}}}\exp(-C^2)\Gamma(C) \tag{1}$$

where $f_o(C)$ is the equilibrium distribution function and

$$\begin{aligned}\Gamma(C) = 1 &+ (q_x C_x + q_y C_y + q_z C_z)(\tfrac{2}{5}C^2 - 1) \\ &- 2(\tau_{x,y}C_xC_y + \tau_{x,z}C_xC_z + \tau_{yz}C_yC_z) \\ &- \tau_{x,x}\left(C_x^2 - C_z^2\right) - \tau_{yy}\left(C_y^2C_z^2\right)\end{aligned} \tag{2}$$

In the work of Garcia and Alder [22], it is shown that

$$q_i = -\frac{k}{P}\left(\frac{2m}{kT}\right)^{\frac{1}{2}}\frac{\partial T}{\partial x_i} \tag{3}$$

$$\tau_{ij} = \frac{\mu}{P}\left(\frac{\partial v_i}{\partial x_j} + \frac{\partial v_j}{\partial x_i} + \frac{2}{3}\frac{\partial v_k}{\partial x_k}\delta_{ij}\right) \tag{4}$$

where q_i and $\tau_{i,j}$ are the dimensionless heat flux and stress tensor, respectively, and subscripts i, j, and k are the Cartesian coordinate indexes.

We substitute the flow parameters obtained from the NS solution into Eqs. (1–4) to estimate the values of coefficients q_i and $\tau_{i,j}$. The values of the q_i and $\tau_{i,j}$ coefficients in the X–Y cross section of the nozzle can be seen in Figs. 2 and 3, respectively. The figures show that the coefficients are largest close to the nozzle wall, due to the formation of the viscous boundary layer. Reference [22] suggests that if the shear stress tensor components and the heat flux coefficients are less than 0.1, then the value of $\Gamma(C)$ in Eq. (1) will be close to unity, and therefore the deviation of the actual distribution from a Maxwellian distribution will be small. This is equivalent to specifying a condition in which the NS equations are applicable. For our application, however, we wish to obtain the appropriate criteria to justify the use of the eDSMC technique and to provide guidelines for which stagnation conditions and geometries may be used for modeling three-dimensional MEMS micronozzles. In our implementation, we may need a smaller critical value of the coefficients to ensure that the deviation from the equilibrium distribution function is indeed small.

Figures 4 and 5 show a comparison of the velocity and temperature profiles along the nozzle centerline obtained by these two different methods. Figures 6 and 7 also show contour plots of temperature and the velocity x component in the X–Y cross section of the nozzle. It can be seen from the figures that the eDSMC predictions correspond to those obtained by the NS solver; the difference between the results is within single percentage points for most parts of the flow. Good agreement is also obtained in the predicted nozzle thrust values of

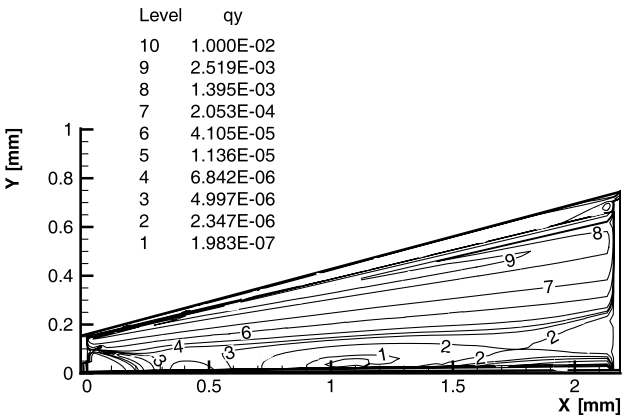

Fig. 2 Case I: NS q_y coefficient; nozzle dimensions are in meters; the supersonic portion of the nozzle starts from the end of the throat ($x = 0.0$ of Fig. 1); the x axis is defined similarly in the subsequent contour figures.

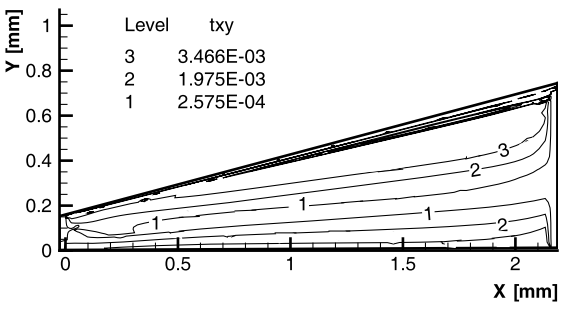

Fig. 3 Case I: NS τ_{xy} coefficient; nozzle dimensions are in meters.

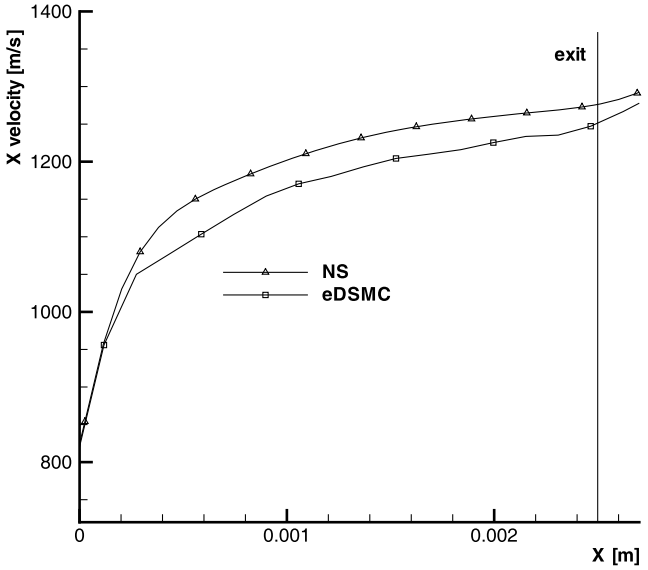

Fig. 4 Case I: NS vs eDSMC, *X* velocity along the nozzle centerline.

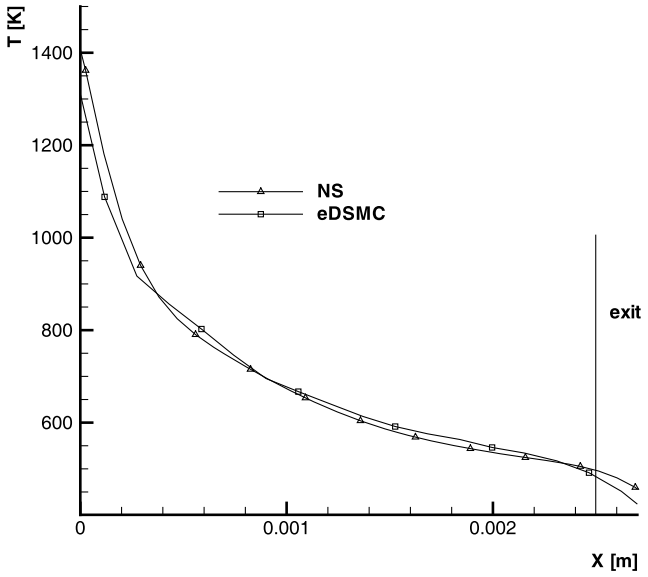

Fig. 5 Case I: NS vs eDSMC, temperature contours along the nozzle centerline.

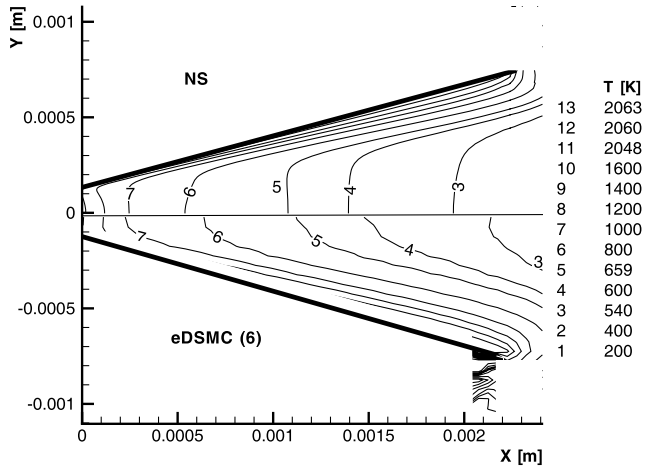

Fig. 6 Case I: NS vs eDSMC, temperature contours; nozzle dimensions are in meters.

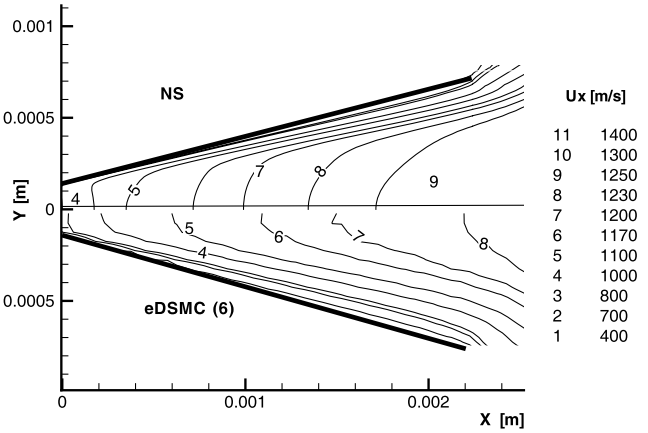

Fig. 7 Case I: NS vs eDSMC, *X* velocity contours; nozzle dimensions are in meters.

0.12 and 0.10 N for NS and eDSMC, respectively. Along with the other results presented in this paper, the results demonstrate the applicability of the eDSMC method to a viscous high-pressure flow that cannot be calculated by baseline DSMC.

IV. Experimental Results and Comparison with eDSMC Simulations

Testing of miniature nozzles was conducted at the NASA John H. Glenn Research Center at Lewis Field (GRC) as a follow-up to the work conducted in [1]. The previous study measured the performance of ambient-temperature nitrogen and helium gas flows through rectangular silicon nozzles, with approximately 250 by 350 μm throats. The nozzle performance (thrust coefficient) was found to peak at area ratios less than 5, but with a secondary performance peak at area ratios above 15.

The follow-up work was concerned with measuring thrust performance with heated gas flows. In this case, nozzles were designed with nominal throat widths of 300 μm, but with depths of 3 and 6 mm. There were a number of reasons for using the larger-scale nozzles. First, the previous work had been done in electric propulsion test facilities, with thrust stands sensitive enough to measure millinewton thrust levels. These facilities would be unavailable for the follow-up work. Rather, the testing would be done in a small rocket facility, with thrust stands able only to measure down to the newton level (it was originally designed for 110-N thrusters). Second, there had been wide dimensional variations in the nozzles, due to difficulty of the etching this design in silicon. It was felt that the larger-scale nozzles would alleviate these concerns and still be relevant to miniature-nozzle optimization trends. The larger nozzles would also make it easier to instrument them with thermocouples, so that the thermal response could be measured.

The nozzles were fabricated from nickel 200, a material with a similar melting point and heat capacity to silicon. Using nickel 200 allows fabrication to be done with conventional metalworking techniques. The nozzles, shown in Fig. 8, were flat rectangular pieces open on either side, with an inlet tube welded to the front. The nozzles were installed in holders that could be clamped onto a fixture, which in turn could be mounted on the thrust stand. The holder had a small hole that aligned with the end of the barrel section of the nozzle to measure chamber pressure. The holder also had type-K thermocouples aligned on either side of the chamber and the throat. The thermocouples were sealed in the holder with a high-temperature cement. When the nozzle was clamped in the holder, the thermocouples contacted the surface of the nozzle. The nozzles were sealed with a thin sheet of flexible graphite on either side.

Dimensional measurements were made with a measuring microscope. The throat and nozzle exit widths and depths were measured before they were installed in the holder. There was a concern that when the nozzles were clamped down in their holders, the soft nickel material was compressing and distorting the

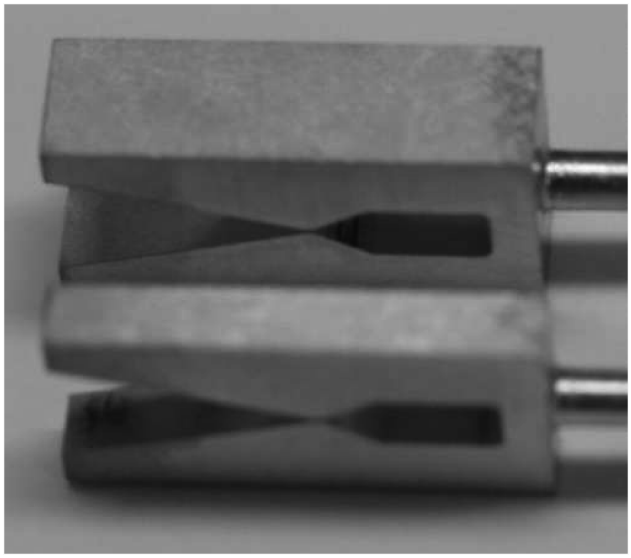

Fig. 8 Cases II–VII: micronozzle shape.

dimensions, and so the nozzles were also dimensioned in their holders.

The nozzle and holder was mounted in a vacuum chamber. A roughing pump typically brought ambient pressures down to around 0.03 atm. The gas flow was controlled with a volumetric flow controller. Testing was conducted over a range of chamber pressures, but primarily between 5 to 7 atm. Two radial line heaters in series were used to heat the nitrogen gas. Nitrogen flows were heated to temperatures up to 900°F at the thruster inlet. Thrust was measured using a 4.45-N compression load cell, mounted in line with the thrust axis. Calibrations were accomplished by suspending 50- and 100-g precision weights from the end of the thrust stand. Thrust calibrations were done at vacuum pressure, with the inlet line pressurized with nitrogen to the inlet valve, before and after each test series. The measurement uncertainty in the thrust measurements was estimated to be ±7%.

The dimensions of studied nozzles are presented in Table 3, and the experimental data for all cases are given in Tables 4–8. The data are also presented in Fig. 9, which shows the thrust coefficient as a function of Reynolds number. There is a clear difference in the thrust coefficient between each of the nozzles, with the lowest values coming from the smallest nozzle (1-A) and the highest values for the largest nozzle (20-A). However, if each nozzle is considered separately, there is very little variation in thrust coefficient with Reynolds number.

Six of the experimental cases, designated as cases II–VII, were chosen for comparison of computations with experiment. The data for these cases are provided in Tables 5 and 6. The selected cases involve two of the nozzles, which are shown in Figs. 10 and 11. The subsonic portion of the nozzle was modeled to provide a better

Table 3 Experimentally studied nozzles

Nozzle type	Depth, mm	Throat area, mm^2	Area ratio
1-A	2.71	0.84	1.00
5-A	2.52	0.60	5.83
10-A	2.49	0.82	9.03
15-A	2.73	0.74	15.33
20-A	2.24	0.74	18.36

Table 4 Experimental data: nozzle 1-A

Test	T_0, K	P_0, atm	Mass flow rate, g/s	Measured thrust, N
1	289.47	5.10	0.926	0.209
2	289.47	5.10	0.926	0.227
3	355.08	5.65	0.926	0.205
4	397.34	5.99	0.926	0.214
5	432.36	6.19	0.926	0.214
6	467.95	6.33	0.907	0.231
7	497.42	6.40	0.888	0.236
8	520.21	6.19	0.849	0.214
9	553.57	6.33	0.849	0.249
10	586.93	6.53	0.849	0.231
11	606.95	5.99	0.753	0.231
12	651.98	6.19	0.753	0.205
13	668.66	6.26	0.753	0.240
14	688.12	6.40	0.753	0.249
15	694.8	6.40	0.753	0.240
16	684.79	5.65	0.676	0.231
17	720.37	5.78	0.676	0.258
18	718.15	5.78	0.676	0.271
19	733.16	6.06	0.695	0.267
20	727.04	5.99	0.695	0.311
21	724.82	5.99	0.695	0.258
22	706.47	5.92	0.695	0.280

Table 5 Experimental data: nozzle 5-A

Test	T_0, K	P_0, atm	Mass flow rate, g/s	Measured thrust, N	Case no.
23	291.7	5.10	0.618	0.383	Case II
24	291.7	5.10	0.618	0.387	
25	333.95	5.51	0.618	0.405	
26	399	5.24	0.540	0.400	Case III
27	453.49	5.51	0.540	0.400	
28	484.07	5.65	0.540	0.405	Case IV
29	533.56	4.97	0.444	0.347	
30	556.35	5.10	0.463	0.351	
31	583.04	5.17	0.463	0.343	Case V
32	606.95	5.24	0.463	0.356	
33	625.3	5.31	0.463	0.365	
34	630.3	5.31	0.463	0.365	
35	598.61	5.24	0.463	0.365	
36	634.75	5.38	0.463	0.365	
37	641.98	5.38	0.463	0.365	
38	656.99	5.44	0.463	0.356	Case VI

Table 6 Experimental data: nozzle 10-A

Test	T_0, K	P_0, atm	Mass flow rate, g/s	Measured thrust, N
39	294.48	4.90	0.926	0.472
40	294.48	4.90	0.926	0.472
41	406.23	5.78	0.926	0.534
42	504.64	5.58	0.791	0.529
43	517.99	5.65	0.791	0.507
44	584.71	5.38	0.714	0.463
45	629.19	5.58	0.714	0.476
46	658.1	5.65	0.714	0.494
47	681.45	5.44	0.676	0.467
48	704.25	5.51	0.676	0.467
49	715.92	5.58	0.676	0.467
50	712.59	5.58	0.676	0.454
51	700.91	5.51	0.676	0.485
52	683.68	5.44	0.676	0.449
53	662.55	5.38	0.676	0.445
54	645.31	5.31	0.676	0.445
55	620.85	5.17	0.676	0.454
56	674.22	5.44	0.676	0.458
57	698.69	5.51	0.676	0.476
58	719.26	5.58	0.676	0.467
59	720.37	5.58	0.676	0.454
60	733.16	5.65	0.676	0.467
61	733.16	5.65	0.676	0.458
62	734.27	5.65	0.676	0.463
63	709.81	5.58	0.676	0.449
64[a]	727.04	5.65	0.676	0.458

[a]This case is case VII.

Table 7 Experimental data: nozzle 15-A

Test	T_0, K	P_0, atm	Mass flow rate, g/s	Measured thrust, N
65	290.58	5.51	0.926	0.431
66	290.58	5.51	0.926	0.423
67	343.4	5.99	0.926	0.467
68	409.57	6.46	0.926	0.512
69	456.83	6.67	0.907	0.525
70	492.41	6.67	0.888	0.503
71	500.75	5.85	0.753	0.454
72	496.3	5.85	0.753	0.449
73	484.07	5.78	0.753	0.449
74	576.37	5.65	0.676	0.427
75	638.08	5.92	0.676	0.423
76	601.94	5.72	0.676	0.436
77	580.82	5.38	0.618	0.400
78	656.99	5.65	0.618	0.409
79	676.45	5.72	0.618	0.423
80	693.68	5.78	0.618	0.418

Table 8 Experimental data: nozzle 20-A

Test	T_0, K	P_0, atm	Mass flow rate, g/s	Measured thrust, N
81	291.7	4.90	0.926	0.498
82	291.7	4.90	0.926	0.507
83	291.7	4.90	0.926	0.512
84	336.18	5.24	0.926	0.543
85	408.46	5.72	0.926	0.596
86	450.71	6.06	0.926	0.609
87	490.19	5.17	0.753	0.525
88	546.9	5.44	0.753	0.547
89	450.71	5.17	0.753	0.507
90	529.66	5.51	0.753	0.538
91	291.7	4.97	0.926	0.529
92	293.36	4.97	0.926	0.480
93	425.14	5.85	0.907	0.614
94	538.56	5.51	0.753	0.560
95	605.84	5.17	0.676	0.525
96	650.87	5.31	0.676	0.512
97	684.79	5.44	0.676	0.520
98	703.14	5.51	0.676	0.520
99	620.85	5.24	0.676	0.520
100	654.76	5.38	0.676	0.520
101	684.79	5.44	0.676	0.520
102	711.48	5.58	0.676	0.525

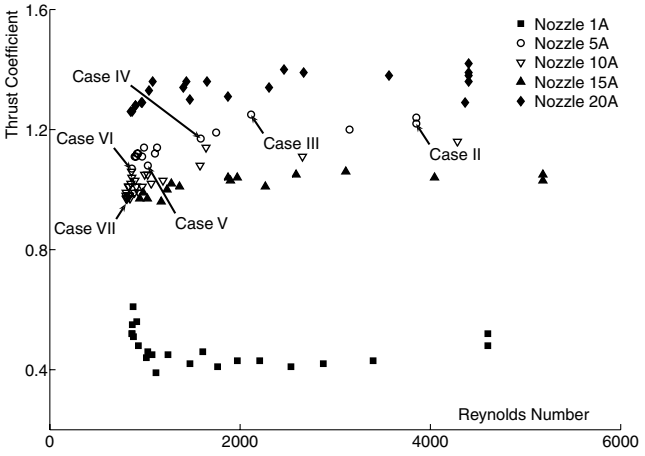

Fig. 9 Experimental data: thrust coefficient as a function of Reynolds number.

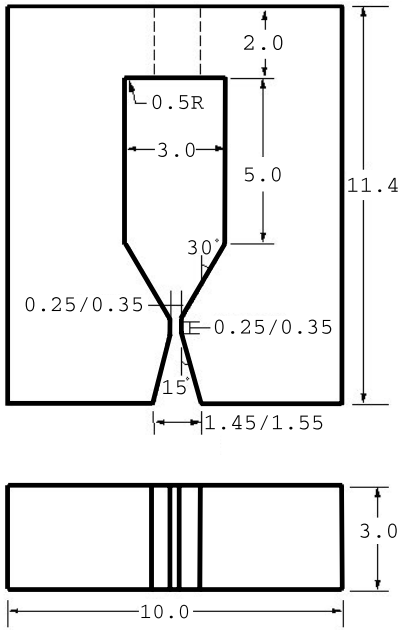

Fig. 10 Cases II–VI: nozzle geometry for type 5-A (mm).

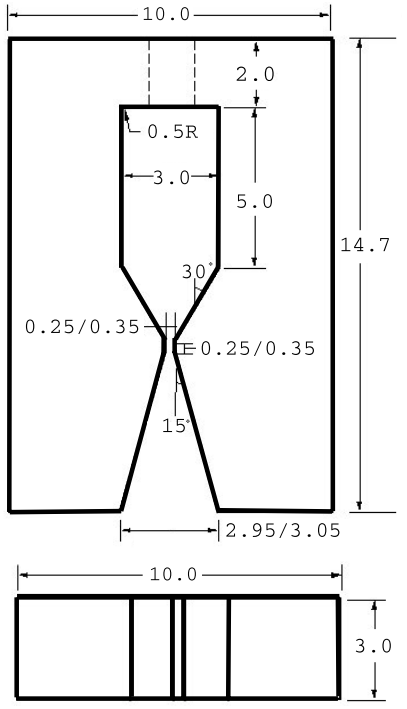

Fig. 11 Case VII: nozzle geometry for type 10-A (mm).

approximation of the flow parameters at the entrance into the supersonic portion of the nozzle (the region of main interest) rather than calculating the sonic boundary conditions at the end of the throat by the isentropic theory. All of the results in this paper present the supersonic portion of the nozzle, starting from the end of the nozzle throat, which is 0.25 mm in length. The simulations performed in this work assume that the background pressure is zero. Using one-dimensional isentropic theory, the percentage change in the thrust coefficient for an exit Mach number of 3 was found to be approximately 4% for the estimated maximum background pressure of 0.03 atm.

A series of eDSMC calculations was performed to validate the method against the experimental data for the nozzle shown in Fig. 10. The flow parameters of the performed cases are shown in Table 1, and the eDSMC scheme parameters are shown in Table 2

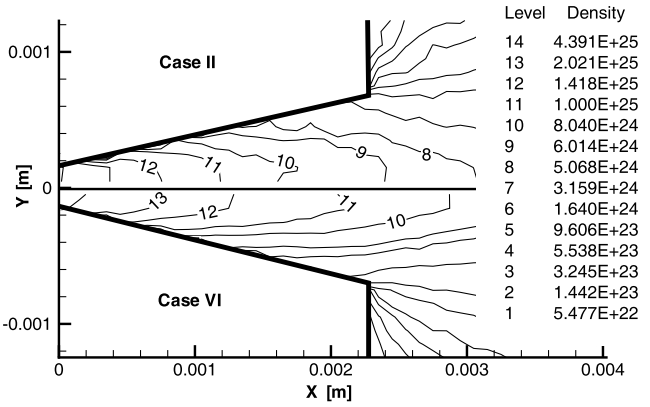

Fig. 12 Cases II and VI: comparison of eDSMC computed density contours (kg/m^3).

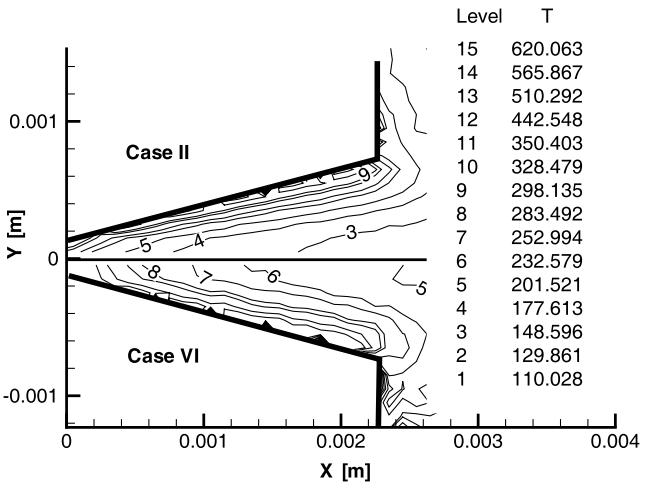

Fig. 13 Cases II and VI: comparison of eDSMC computed temperature contours (K).

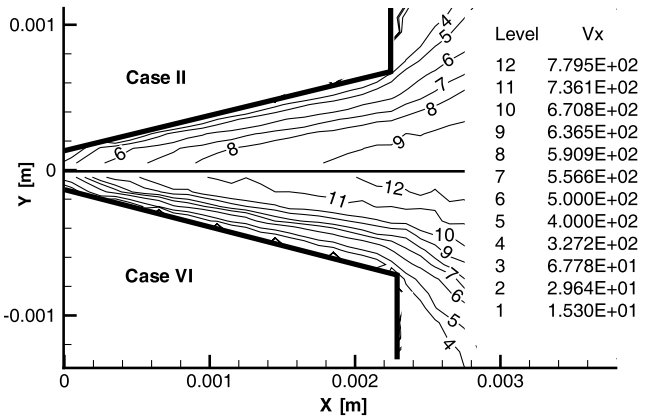

Fig. 14 Cases II and VI: comparison of eDSMC computed *X* velocity contours (m/s).

(cases II–VII). As can be seen from Table 2, Cases II–VII use a smaller number of computational particles and cells than the higher-temperature case I. The reduced set of computational parameters is due to the lower viscosity for these cases compared with case I. In that case, the stagnation temperature is several times higher for a similar stagnation-pressure value. The lower stagnation temperatures for cases II–VII, as well as the thicker nozzle throat height (a factor of 2 higher than case I), reduce the overall region of the flow in which the viscous boundary layer will be important. In addition, for case II, we

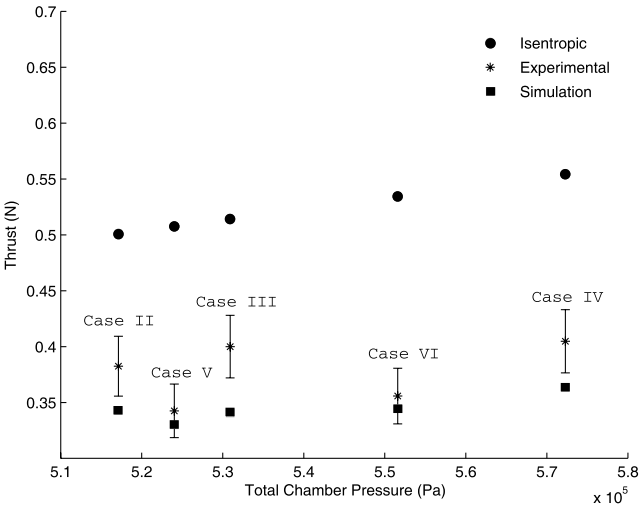

Fig. 15 Cases II–VI: comparison of experimental and computed thrust as a function of chamber stagnation pressure for the case 5-A nozzle.

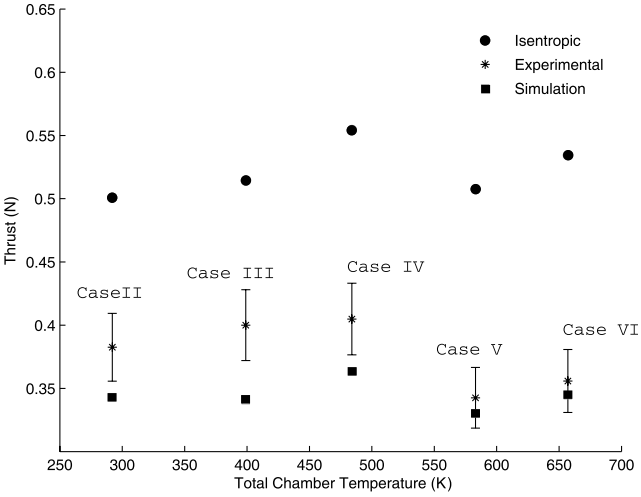

Fig. 16 Cases II–VI: comparison of experimental and computed thrust as a function of stagnation temperature for the case 5-A nozzle.

checked the convergence of the eDSMC solution with respect to the number of computational particles and cells and found that when the number was decreased by a factor of 2, the flowfield and thrust remained essentially the same.

Figures 12–14 show the comparison of the density, temperature, and *X*-component velocity contours calculated with eDSMC for the least (case II) and most viscous case (case VI) of nozzle type 5-A. Case II has the highest Reynolds number and the lowest temperature, whereas case VI has the lowest Reynolds number and highest temperature. As can be seen in Table 5, the nozzle thrust for these two different cases is the same, which means that the increase in the stagnation temperature from 292 to 657 K does not produce the expected increase in the thrust, whereas it adversely increases the thermal load on the nozzle wall. The efficiency of the higher-temperature nozzle is lower due to the larger viscous loses at the lower Reynolds number. Moreover, it can be seen in Figs. 12–14 that the flow in the supersonic part of the nozzle for both cases is dominated by viscous effects, which produces a thick boundary layer occupying the entire supersonic portion of the nozzle. This is why a higher stagnation temperature does not translate into better performance of the nozzle. These computational results are used to compute the predicted thrust levels presented in Figs. 15 and 16, which were seen to be consistent with measured values and mostly within experimental error bars. The small residual difference between modeling and experiment may be due to limitations in the eDSMC method or unaccounted errors in the experiment or both.

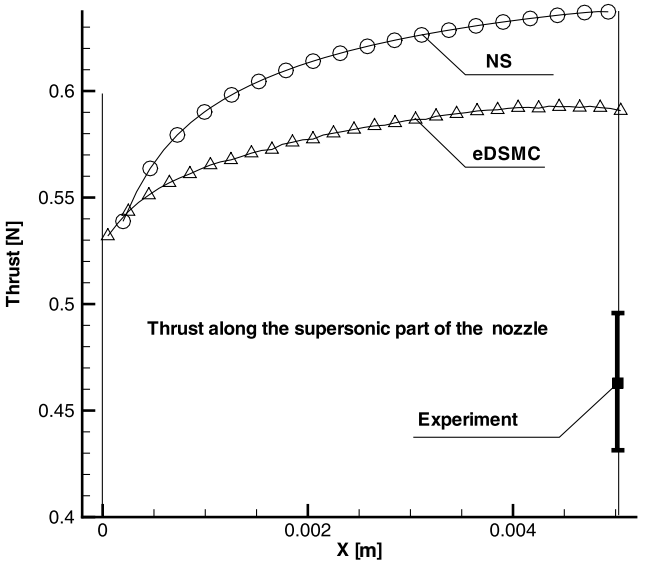

Fig. 17 Case VII: comparison of computational and experimental thrust profiles along the nozzle centerline for case VII.

Because we will subsequently discuss possible additional experimental error sources, let us consider here possible limitations in the eDSMC method. It should be noted that eDSMC cannot capture the viscous effects as precisely as Bhatnagar–Gross–Krook (BGK) schemes such as those discussed by Burt and Boyd [23] or Gallis and Torczynski [24], because the ad hoc assumption of local equilibrium reduces dissipative properties of the flow. Although these schemes may be more exact than the eDSMC scheme, they are more complex to implement and could be computationally intractable for these highly three-dimensional flows considered here. The eDSMC flow solutions, however, clearly show the establishment of the boundary layer sufficiently well to provide good agreement with the experiment.

The second nozzle, presented in Fig. 11, was studied with both the eDSMC and NS techniques. The flow geometry of the performed case is given in Table 1, and the eDSMC scheme parameters are shown in Table 2 (case VII). It should be noted that this case is more challenging for both methods because of the long nozzle length, which allows greater growth of the viscous boundary layer. The thrust predicted by the NS solver and eDSMC and obtained from the experiment for this case is 0.63, 0.59, and 0.46 N, respectively. Figure 17 presents the thrust increase along the supersonic part of the nozzle. It can be seen in the figure that the length of the diverging part

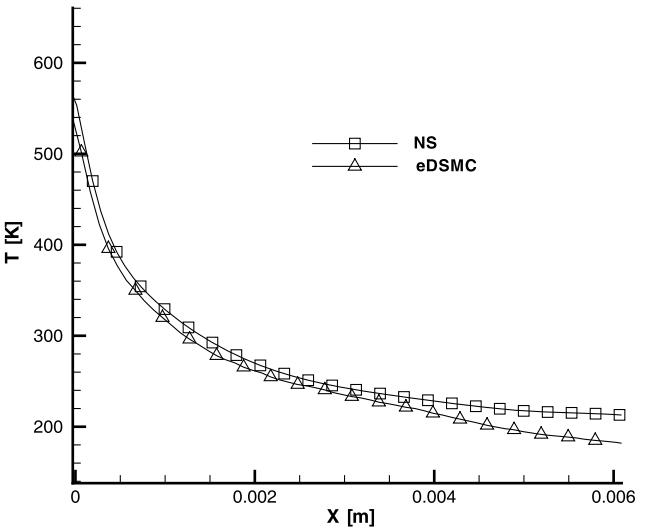

Fig. 18 Case VII: computed temperature along the centerline.

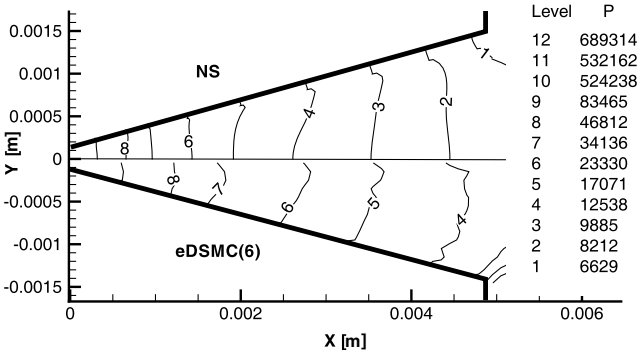

Fig. 19 Case VII: computed pressure contours (Pa).

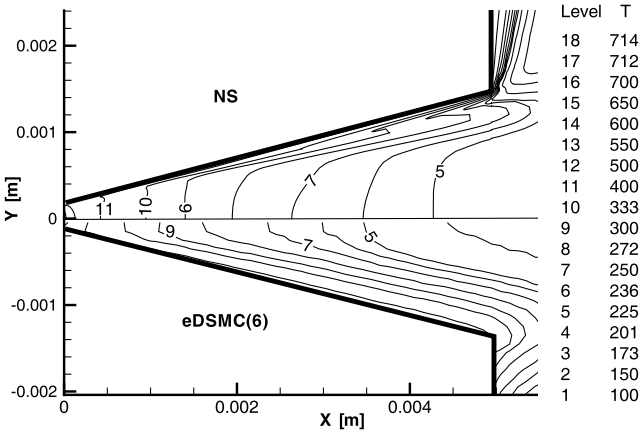

Fig. 20 Case VII: computed temperature contours (K).

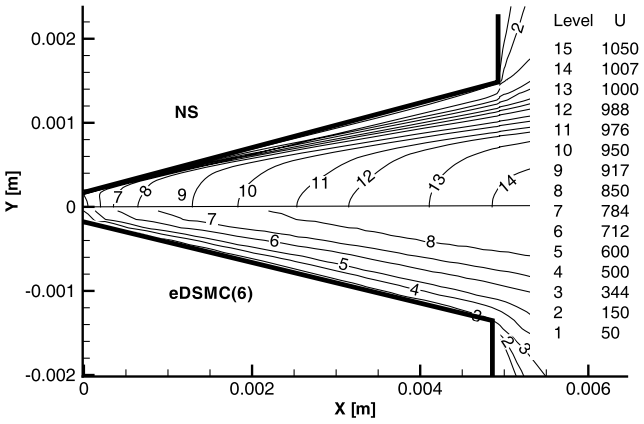

Fig. 21 Case VII: computed *X*-component velocity contours (m/s).

of the nozzle is optimum and that any further increase in the length would probably not improve the device performance. The comparison between the NS and eDSMC flow results for this case, shown in the Figs. 14–21, suggests that both computational methods are in reasonable agreement, with the NS solution being considered the "exact" solution. It may be seen that the thrust predicted by both methods agrees approximately within 6%. The eDSMC solution predicts a *more* viscous boundary-layer formation than NS, however. This seemingly contradictory result has been discussed in the work of Breuer et al. [25] as well as Xu et al. [26], who recognized that kinetic models may sometimes give results that are more diffusive than those obtained from traditional high-resolution difference schemes. This problem will become important for eDSMC applications to higher stagnation-pressure micronozzle flows, because the cell size (for both DSMC and eDSMC) must be small enough to match the higher gradients in the thinner boundary layer [13]. Alternative forms of grid adaptation beyond what is present in the SMILE computational

tool [27] will need to be developed, but this is beyond the scope of this work.

The experimental value of the nozzle thrust in this case is significantly lower for either computational method and, based on the preceding discussion, the apparent better agreement with eDSMC is probably fortuitous. Difficulties in simultaneously measuring the nozzle thrust and throat-area dimension most likely introduced additional errors that are difficult to quantify. The nozzle and holder had to be mounted on the microscope with the thin inlet tube and its fitting facing the table, making it difficult to get light to the throat. Also, the weight of the thermocouple connectors and pressure tap could have caused the nozzle and holder to be leaning slightly, so that the microscope was not viewing a flat surface. With the equipment available to mount the holder, an unknown bias error to the measurements of the nozzles installed in the holders may have been introduced. If this is the case, both computational methods will be sensitive to this experimental uncertainty in the throat geometry for longer nozzles. This comparison between high-fidelity flow modeling and careful experimental research highlights the experimental challenges and requirements for future microthruster measurements.

V. Conclusions

The modeling and simulation of three-dimensional micronozzle flows in the 200 to 2000 Reynolds number regime is challenging due to the multiple length scales present in the flow and the large viscous boundary layer. The nature of the flows makes it difficult for a single computational method, DSMC or NS, to adequately represent the physics of the flow. A new collision-limiter method, designated as eDSMC, that extends the direct simulation Monte Carlo (DSMC) technique to high-pressure flows is presented and applied to realistic three-dimensional micronozzle thrusters. The proposed method is based on the idea that local equilibrium may be assumed to have occurred after a fixed number of collisions per time step per cell, for which the number of collisions required to obtain equilibrium is determined in separate presimulation testing. Chapman–Enskog theory was used to predict the applicability of eDSMC for the nozzle configurations presented in this work.

The eDSMC method was tested against a NS computation for a three-dimensional nozzle with high stagnation pressure and temperatures, and good agreement was obtained for a condition that may not be modeled with the usual DSMC method. Comparisons of eDSMC predictions of nozzle thrust with a new experiment were also presented and found to be in good agreement for a three-dimensional nozzle with an area ratio on the order of 5. Thrust levels predicted as a function of stagnation pressure and temperature followed experimental trends and generally fell within the experimental error bars. The data and simulations showed that the efficiency of the higher-temperature nozzle is lower due to larger viscous losses at lower Reynolds numbers. Navier–Stokes and eDSMC calculations were also performed for a second micronozzle with an area ratio of nine. Both simulation methods agreed well with each other; however, it is likely that the eDSMC calculations exhibit a small amount of artificial viscosity in the modeling of the high gradients in the boundary layer. Both simulation predictions of thrust overpredict the experiment, which suggests that there may be additional experimental errors in the measurement of the actual nozzle-throat-region dimensions that are difficult to quantify. The importance of obtaining simultaneously accurate thrust as well as nozzle configuration measurements is highlighted by this comparison and encourages the development of additional techniques to enable future measurements for realistic micronozzle geometries.

Acknowledgments

The research performed at Pennsylvania State University was supported by the U.S. Air Force Office of Scientific Research grant no. F49620-02-1-0104, administered by Mitat Birkan.

References

[1] Reed, B. D., De Groot, W., and Dang, L., "Experimental Evaluation of Cold Flow Micronozzles," AIAA Paper 2001-3521, July 2001.

[2] Mueller, J., Chakraborty, I., Bame, D., and Tang, W., "Vaporizing Liquid Microthruster Concept: Preliminary Results of Initial Feasibility Studies," *Micropropulsion for Small Spacecraft*, edited by Micci, M., and Ketsdever, A., Progress in Astronautics and Aeronautics, Vol. 187, AIAA, Reston, VA, 2000, pp. 215–230.

[3] Ketsdever, A. D., Glabough, M. T., Gimelshein, S., and Alexeenko, A., "Experimental and Numerical Determination of Micropropulsion Device Efficiencies at Low Reynolds Numbers,"*AIAA Journal*, Vol. 43, No. 3, Mar. 2005.

[4] Bayt, R. L., Breuer, K. S., Lin, L., Forster, F. K., Aluru, N. R., and Zhang, X., "Viscous Effects in Supersonic MEMS Fabricated Micronozzles," *1998 ASME International Mechanical Engineering Congress and Exposition (MEMS-1998)*, American Society of Mechanical Engineers, New York, 1998, pp. 117–123.

[5] Chen, K., Winter, M., and Huang, R. F., "Supersonic Flow in Miniature Nozzles of the Planar Configuration," *Journal of Micromechanics and Microengineering*, Vol. 15, No. N9, 2005, pp. 1736–1744. doi:10.1088/0960-1317/15/9/016

[6] Zelesnik, D., Micci, M., and Long, L., "Direct Simulation Monte Carlo Model of Low Reynolds Number Nozzle Flows," *Journal of Propulsion and Power*, Vol. 10, No. 4, 1994, pp. 546–553.

[7] Chung, C. H., Kim, S., Strubbs, R., and De Witt, K., "Low-Density Nozzle Flow by the Direct Simulation Monte Carlo and Continuum Methods," *Journal of Propulsion and Power*, Vol. 11, No. 1, 1995, pp. 64–78.

[8] Alexeenko, A., Levin, D., Gimelshein, S., Collins, R., and Reed, B., "Numerical Modeling of Axisymmetric and Three-Dimensional Flows in MEMS Nozzles," *AIAA Journal*, Vol. 40, No. 5, 2002, pp. 897–904.

[9] Alexeenko, A. A., Levin, D. A., Fedosov, D. A., and Gimelshein, S. F., "Coupled Thermal-Fluid Modeling of Micronozzles for Performance Analysis," *Journal of Microelectromechanical Systems*, May 2005 (submitted for publication).

[10] Alexeenko, A., Fedosov, D., Levin, D., Gimelshein, S., and Collins, R. J., "Performance Analysis of Microthrusters Based on Coupled Thermal-Fluid Modeling and Simulation," *Journal of Propulsion and Power*, Vol. 21, No. 1, 2005, pp. 95–101.

[11] Titov, E. V., Zeifman, M. I., and Levin, D. A., "Examination of New DSMC Methods for Efficient Modeling of MEMS Device Flows," 4th AIAA Theoretical Fluid Mechanics Meeting, Toronto, Ontario, AIAA Paper 2005-5058, 6–9 June 2005.

[12] Lengrand, J. C., Raffin, M., Allegre, J., and Hughes, R. D. *Monte-Carlo Simulation Method Applied to Jet Wall Interactions Under Continuum Flow Conditions*, Rarefied Gas Dynamics, Vol. 74, AIAA, New York, 1981, pp. 994–1006.

[13] Titov, E., and Levin, D., "Extension of the DSMC Method to Higher Pressure Flows," *International Journal of Computational Fluid Dynamics* (submitted for publication).

[14] Titov, E., "Application of the DSMC Method to High Density Micro-Flows," Ph.D. Thesis in Aerospace Engineering, Pennsylvania State Univ., University Park, PA, Aug. 2007.

[15] Bird, G. A., *Molecular Gas Dynamics and the Direct Simulation of Gas Flows*, Clarendon Press, Oxford, 1994.

[16] Pullin, D. I., "Direct Simulation Methods for Compressible Inviscid Ideal-Gas Flow," *Journal of Computational Physics*, Vol. 34, Feb. 1980, pp. 231–244. doi:10.1016/0021-9991(80)90107-2

[17] Macrossan, M. N., Metchnik, M. V., and Pinto, P. A., "Hypersonic Flow over a Wedge with a Particle Flux Method," *24th International Symposium on Rarefied Gas Dynamics*, Vol. 762, American Inst. of Physics, Melville, NY, 2005, pp. 650–655.

[18] Sharma, A., and Long, L. N., "A Parallel Object-Oriented DSMC Method for Blast-Impact Simulations," 16th AIAA Computational Fluid Dynamics Conference, Orlando, FL, AIAA Paper 2003-4234, June 2003.

[19] "General Aerodynamic Simulation Program, Computational Flow Analysis Software for the Scientist and Engineer," *Gasp Ver. 3, User's Manual*, Aerosoft Co., Blacksburg, VA, May 1996.

[20] Titov, E. V., Zeifman, M. I., and Levin, D. A., "Application of the Kinetic and Continuum Techniques to the Multi-Scale Flows in MEMS Devices," 43rd AIAA Aerospace Science Meeting, Reno, NV, AIAA Paper 2005-1399, 10–13 Jan. 2005.

[21] "Gridgen User Manual," Ver. 14.05, Pointwise, Inc., Fort Worth, TX, 1999.

[22] Garcia, A. L., and Alder, B. J., "Generation of the Chapman–Enskog Distribution," *Journal of Computational Physics* Vol. 140, No. 1,

Feb. 1998, pp. 66–70.
doi:10.1006/jcph.1998.5889
[23] Burt, J. M., and Boyd, I. D., "Evaluation of a Particle Method for the Ellipsoidal Statistical Bhatnagar–Gross–Krook Equation," 44th AIAA Aerospace Science Meeting and Exhibit, Reno, NV, AIAA Paper No. 2006-989, Jan. 2006.
[24] Gallis, M. A., and Torczynski, J. R., "The Application of the BGK Model in Particle Simulations," 34th AIAA Thermophysics Conference, Denver, CO, AIAA Paper No. 2000-2360, June 2000.
[25] Breuer, K. S., Piekos, E. S., and Gonzales, D. A., "DSMC Simulations of Continuum flows," Thermophysics Conference, 30th, San Diego, CA, AIAA Paper AIAA-1995-2088, 19–22 June 1995.
[26] Xu, K., Martinelli, L., and Jameson, A., "Gas-Kinetic Finite Volume Methods, Flux-Vector Splitting, and Artificial Diffusion," *Journal of Computational Physics*, Vol. 120, No. 1, Aug. 1995, pp. 48–65.
doi:10.1006/jcph.1995.1148
[27] Ivanov, M. S., Markelov, G. N., and Gimelshein, S. F., "Statistical Simulation of Reactive Rarefied Flows: Numerical Approach and Application," AIAA Paper 98-2669, June 1998.

E. Choueiri
Associate Editor